An extended boundary element method formulation for the direct calculation of the stress intensity factors in fully anisotropic materials

Authors: Gabriel Hattori, Ibrahim A. Alatawi and Jon Trevelyan
School of Engineering and Computing Sciences, Durham University,
Durham, DH1 3LE, UK.
E-mail: gabriel.hattori@durham.ac.uk

ABSTRACT

We propose a formulation for linear elastic fracture mechanics (LEFM) in which the stress intensity factors (SIF) are found directly from the solution vector of an extended boundary element method (XBEM) formulation. The enrichment is embedded in the BEM formulation, rather than adding new degrees of freedom for each enriched node. Therefore, a very limited number of new degrees of freedom is added to the problem, which contributes to preserving the conditioning of the linear system of equations. The Stroh formalism is used to provide BEM fundamental solutions for any degree of anisotropy, and these are used for both conventional and enriched degrees of freedom. Several numerical examples are shown with benchmark solutions to validate the proposed method.

Keywords: extended boundary element method; implicit enrichment; fracture mechanics; anisotropic materials; Stroh formalism

1 Introduction

Enriched formulations have been studied over 15 years since the partition of unity (PU) method [1] was first employed in the finite element method framework [2, 3] to model cracks through additional degrees of freedom that capture the asymptotic behaviour of the displacement around the crack tip. This approach has allowed engineers to achieve more accurate displacement solutions at the crack surface using coarser meshes than conventional finite element formulations, and also liberated crack growth simulations from the requirement to remesh since the crack may pass through elements. This approach was named extended finite element method (XFEM), and the development of enrichment functions remains a topic of considerable interest [4, 5, 6, 7, 8].

With its high accuracy of boundary solutions and ability to capture discontinuous solution fields, the boundary element method (BEM) has been

a tool of choice for decades in linear elastic fracture mechanics. Since the discretisation is applied only to the boundaries in BEM, the crack surface is still part of the geometry. The PU has been shown to be applicable within a BEM framework [9, 10], and its convergence properties shown to outperform conventional BEM formulations.

The main inconvenience of the enriched formulations is that the number of additional degrees of freedom may affect the solution since it might cause ill-conditioning of the system of linear equations. For instance, Laborde et al. [11] have analysed different enrichment approaches and compared how the conditioning degrades with each. Fixed area enrichment around the crack (geometrical enrichment) has been shown to improve the overall results of the analysis [12]. However, it can be very sensitive to the number of enriched degrees of freedom with crack tip enrichment functions. A high number will lead to an ill-conditioned system of equations. This characteristic is the main deficiency in XFEM formulations. One can verify that the conditioning can degrade quite rapidly depending of the enrichment approach employed. Béchet et al. [13] have used preconditioners to improve the conditioning of the system. In this paper, we define the enrichment strategies used in XFEM as explicit enrichment.

An alternative to the use of explicit enrichment is to embed the enrichment into the formulation. This approach can be defined as implicit enrichment, and the main advantage is to allow the direct calculation of the Stress Intensity Factors (SIF) without the need of post-processing such as the J-integral.

Several authors have studied different methodologies to evaluate the SIFs. Liu et al. [14] have used the leading and high order terms of the asymptotic displacements around the crack tip using the partition of unity. To enforce that the displacements converge to the actual asymptotic fields around the crack tip, the actual displacements around the crack tip are set to zero. The displacements around the crack tip can be expressed using an expression for the asymptotic fields and the SIFs. Hence, the SIFs can be obtained without the need for post-processing the displacements. Xiao et al. [15] have used a hybrid crack element to calculate the SIFs of mixed mode cracks without any post-processing.

Weak-form displacement and traction integral equations are used to model 3D fracture mechanics problems in BEM by [16]. A special crack tip element is introduced, while making the relative displacements vanish on the crack front. The remaining degrees of freedom for the nodes on the crack front are directly associated with the SIFs.

Watson [17] has proposed singular boundary elements for modelling straight and curved cracks combining Hermitian interpolation functions and singular shape functions which come from the Williams expansion. In this scheme, the singular functions extend over many boundary elements on each crack surface. The SIFs are calculated from the crack opening dis-

placements and the singular functions.

A new singularity subtraction technique is introduced by [18], where the first term of the Williams expansion is used as a regularisation parameter. Using this strategy, the SIFs become unknowns of the BEM problem. Hence, the displacements around the crack tip are enforced to be equal to those predicted by the leading order term in the Williams expansion, so that the problem can be solved.

Recently, Alatawi and Trevelyan [19] have implemented a direct method approach, where the SIFs are part of the unknown variables of the problem rather than a parameter obtained after the solution is known. In this case, the leading order term in the Williams expansion is also used to model the asymptotic behaviour around the crack tip.

All the previous works have tackled the direct evaluation of SIFs for isotropic materials. The objective of this work is to extended the work of [19] to a more general range of materials. Anisotropic materials have been extensively used in the aerospace and automobile industries, and more recently for the study of geological materials applied to the hydraulic fracturing problem. The Stroh formalism is used to provide the necessary anisotropic enrichment functions, in the same way as performed in [12]. The advantage of the Stroh formalism is a concise enrichment function which depends only on the material properties.

The remainder of this paper is organised as follows: in Section 2, the constitutive equations for elastic problems are presented. The BEM formulation and the Stroh formalism are explained in detail in Section 3. The direct approach is tackled in Section 4. Section 5 presents several numerical results to validate the proposed method. We conclude with some final remarks in Section 6.

2 Constitutive equations

Let $\Omega \subset \mathbb{R}^2$ be a fully anisotropic elastic domain; the static equilibrium equations in the absence of body forces are stated as

$$\sigma_{ij,j} = 0 \tag{1}$$

The linear constitutive equations are given by the generalized Hooke's law

$$\sigma_{ij} = C_{ijkl}\varepsilon_{kl} \tag{2}$$

where $\boldsymbol{\sigma}$ is the stress tensor, $\boldsymbol{\varepsilon}_{ij}$ is the strain tensor and C_{ijkl} defines the elastic stiffness tensor. In the case of an anisotropic material, the number of unique elements in the C_{ijkl} tensor also determines the type of symmetry of the material.

Let us remark that the elastic stiffness tensor satisfies the following symmetry relations

$$C_{ijkl} = C_{jikl} = C_{ijlk} = C_{klij} \tag{3}$$

The strain tensor ε_{ij} is defined as

$$\varepsilon_{ij} = \frac{1}{2}(u_{i,j} + u_{j,i}) \tag{4}$$

where u_i stands for the displacements. It is important to remark that the stress and strain tensors also exhibit symmetry properties, i.e.

$$\sigma_{ij} = \sigma_{ji} \tag{5}$$

$$\varepsilon_{ij} = \varepsilon_{ji}, \tag{6}$$

3 The dual boundary element method (DBEM)

The BEM emerged in the 1960s as an alternative for domain discretisation methods such as the finite element method (FEM). It gained popularity from the 1970s, as engineers found its boundary-only discretisation very attractive, since the number of degrees of freedom of the problem were reduced. Moreover, it has been shown in different works of fracture mechanics problems that BEM models can be more accurate and stable than FEM models, which tend to suffer from instabilities arising of highly deformed elements at the crack tips.

Figure 1 illustrates a typical fracture mechanics problem in which an anisotropic elastic body containing a crack is subject to an arbitrary loading. We seek the solution to general problems in elastostatics in terms of the boundary displacements, u_j, and tractions, p_j. For LEFM problems we also seek the SIFs at any crack tips located in Ω. Conventional collocation BEM formulations fail for this problem because the coincident nodes on the opposing crack surfaces give rise to a degeneracy in the resulting linear system of equations. Of the different approaches proposed to circumvent this problem, the most popular is the Dual Boundary Element Method (DBEM).

In the dual BEM formulation, two boundary integral equations (BIEs) are necessary. The displacement boundary integral equation (DBIE) is defined as

$$c_{ij}(\xi)u_j(\xi) + \fint_\Gamma p^*_{ij}(\zeta,\xi)u_j(\zeta)d\Gamma(\zeta) = \int_\Gamma u^*_{ij}(\zeta,\xi)p_j(\zeta)d\Gamma(\zeta), \qquad \xi \in \Gamma \tag{7}$$

where Γ denotes all the boundaries of the problem including crack surfaces Γ_+ and Γ_- of domain Ω; $\fint$ stands for the Cauchy Principal Value integration; c_{ij} is the free term deriving from the Cauchy Principal Value

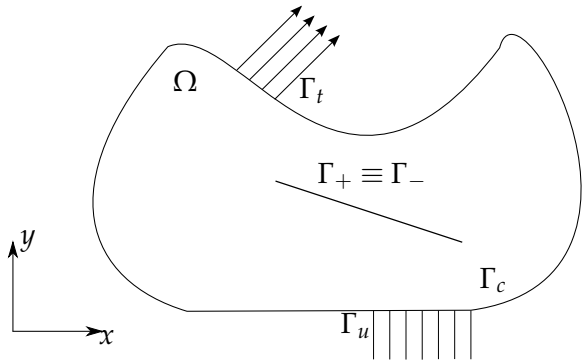

Figure 1: Crack problem in anisotropic material.

integration of the strongly singular kernels p^*_{ij}; u^*_{ij} and p^*_{ij} are the displacement and traction fundamental solutions, respectively, and are detailed in the next section.

In order to overcome the degeneracy in the linear system, a traction boundary integral equation (TBIE) is obtained from the differentiation and further substitution into Eq. (2) of the kernels u^*_{ij} and p^*_{ij}, resulting into two new kernels d^*_{kij} and s^*_{kij}. The TBIE is given by

$$c_{ij}(\boldsymbol{\xi})p_j(\boldsymbol{\xi}) + N_k \fint_\Gamma s^*_{kij}(\boldsymbol{\zeta},\boldsymbol{\xi})u_j(\boldsymbol{\zeta})d\Gamma(\boldsymbol{\zeta}) = N_k \fint_\Gamma d^*_{kij}(\boldsymbol{\zeta},\boldsymbol{\xi})p_j(\boldsymbol{\zeta})d\Gamma(\boldsymbol{\zeta}), \qquad \boldsymbol{\xi} \in \Gamma \tag{8}$$

where $\fint$ stands for the Hadamard Finite Value integration and N_k is the k component of the outward unit normal to the boundary at the collocation point $\boldsymbol{\xi}$.

3.1 Fundamental solutions and the Stroh formalism

The u^*_{ij} and p^*_{ij} kernels are given in terms of the Stroh formalism by [20, 21]

$$u^*_{ij} = -\frac{1}{\pi}\Re\left\{A_{jm}Q_{mi}\,\ln(z^\zeta_m - z^\xi_m)\right\} \tag{9}$$

$$p^*_{ij} = \frac{1}{\pi}\Re\left\{B_{jm}Q_{mi}\,\frac{\mu_m n_1 - n_2}{z^\zeta_m - z^\xi_m}\right\} \tag{10}$$

where $\boldsymbol{n} = (n_1, n_2)$ is the unit normal at the observation point; $z^\zeta_m = \zeta_1 + \mu_m\zeta_2$, $z^\xi_m = \xi_1 + \mu_m\xi_2$ are evaluated at the observation and collocation points, respectively; $\Re$ denotes the real part ; $\mathbf{Q} = \mathbf{A}^{-1}(\mathbf{L}^{-1} + \overline{\mathbf{L}}^{-1})^{-1}$ with $\mathbf{L} = i\mathbf{A}\mathbf{B}^{-1}$ and $\overline{L}$ represents the complex conjugate of L.

After substitution of Eqs. (9) and (10) into Eq. (2), we obtain the follow-

ing relations

$$d^*_{kij} = \frac{C_{kilr}}{\pi} \Re \left\{ A_{jm} Q_{ml} \, \frac{\delta_{r1} + \mu_m \delta_{r2}}{z^\zeta_m - z^\xi_m} \right\} \tag{11}$$

$$s^*_{kij} = \frac{C_{kilr}}{\pi} \Re \left\{ B_{jm} Q_{ml} \, \frac{(\mu_m n_1 - n_2)(\delta_{r1} + \mu_m \delta_{r2})}{(z^\zeta_m - z^\xi_m)^2} \right\} \tag{12}$$

The matrices $\mathbf{A}$, $\mathbf{B}$ and constant μ_m are parameters from the Stroh formalism [22, 23] and can be obtained through solution of the following eigenvalue problem

$$\left(\begin{array}{c|c} -\mathbf{C_{2ij2}}^{-1}\mathbf{C_{2ij1}} & -\mathbf{C_{2ij2}}^{-1} \\ \hline \mathbf{C_{1ij1}} - \mathbf{C_{2ij1}}^T\mathbf{C_{2ij2}}^{-1}\mathbf{C_{2ij1}} & -\mathbf{C_{2ij1}}^T\mathbf{C_{2ij2}}^{-1} \end{array} \right) \left(\frac{\mathbf{A}_m}{\mathbf{B}_m} \right) = \mu_m \left(\frac{\mathbf{A}_m}{\mathbf{B}_m} \right) \tag{13}$$

where there is no summation on the m index.

The calculated eigenvalues are complex numbers, and μ_m will take only the eigenvalues with positive imaginary part. For anisotropic materials, the eigenvalues are always different ($\mu_1 \neq \mu_2$ for 2D problems). However, if this approach is used to model an isotropic material, we have $\mu_1 = \mu_2$, the eigenvectors are not unique, and some special assumptions must be taken into account [22, 23].

3.2 Regularisation of the singular integrands

The kernel u^*_{ij} of Eq. (7) presents a logarithmic singularity, which can be easily regularised by applying a special quadrature for the logarithm. This approach was employed in the works of [20, 24], for instance. Another method to regularise the weakly singular integral is to use the Telles transformation [25], where the singularity is cancelled by the Jacobian of a coordinate transformation, allowing the integral to be evaluated using Gauss-Legendre quadrature.

The kernels p^*_{ij} and d^*_{kij} present strong singularities of order $\mathcal{O}(1/r)$. Finally, the kernel s^*_{kij} presents a hypersingularity of order $\mathcal{O}(1/r^2)$. To evaluate the singular integrals containing these kernels, we use the method employed by Guiggiani and Casalini in [26] initially for 2D BEM elasticity problems and extended to hypersingularities in [27, 28]. This approach has the advantage to be used for singularities of order $\mathcal{O}(1/r^n)$ and consists in expanding the shape functions and Jacobian components in Taylor series in the same way as in the work of Aliabadi et al. [29].

When Eq. (8) is discretised, the hypersingular integral it contains can be rewritten as

$$\int_{-1}^{+1} s_{kij}(\zeta,\xi)^* N^a(\zeta) J(\zeta) d\zeta = \int_{-1}^{+1} G(\zeta,\xi) d\zeta \tag{14}$$

where $N^a(\zeta)$ represents the shape function for node a and $J(\zeta)$ is the Jacobian. We seek to express the integrand in the following form

$$G(\zeta,\xi) = G_0(\zeta,\xi) + \frac{G_{-1}(\xi)}{\zeta-\xi} + \frac{G_{-2}(\xi)}{(\zeta-\xi)^2} \tag{15}$$

where the singularities $\zeta-\xi$ and $(\zeta-\xi)^2$ become explicit, and G_0 is a regular function with the singularities removed.

Adding and subtracting this description of the singularities yields

$$\int_{-1}^{+1} G(\zeta,\xi)\,d\zeta = \int_{-1}^{+1} G_0(\zeta,\xi)\,d\zeta + \fint_{-1}^{+1} \frac{G_{-1}(\xi)}{\zeta-\xi}\,d\zeta + \fint_{-1}^{+1} \frac{G_{-2}(\xi)}{(\zeta-\xi)^2}\,d\zeta \tag{16}$$

The hypersingular integral has been rewritten as the sum of a regular integral that can be evaluated using Gauss-Legendre quadrature, and singular and hypersingular integrals that can be taken analytically. Since the numerator of both integrands is a constant that does not depend on ζ, the solution of the singular integrals can be easily calculated as

$$\fint_{-1}^{+1} \frac{G_{-1}(\xi)}{\zeta-\xi}\,d\zeta = G_{-1}(\xi)\ln\left|\frac{1-\xi}{-1-\xi}\right| \tag{17}$$

$$\fint_{-1}^{+1} \frac{G_{-2}(\xi)}{(\zeta-\xi)^2}\,d\zeta = G_{-2}(\xi)\left(\frac{1}{-1-\xi} - \frac{1}{1-\xi}\right) \tag{18}$$

To calculate $G_{-1}(\xi)$ and $G_{-2}(\xi)$ we follow the works of Guiggiani [27, 28]. The elements of Eq. (14) can be expressed in terms of their Taylor series expansion around the singular point, which occurs when $\xi \to \zeta$. The expansion of the shape functions in Taylor series is given by

$$N^a(\zeta) = N^a(\xi) + \left.\frac{dN^a(\zeta)}{d\zeta}\right|_{\zeta=\xi} \lambda + \mathcal{O}(\lambda^2) \tag{19}$$

where $\lambda = \zeta - \xi$. The Jacobian has to be multiplied by the normal components n_1 and n_2 before a Taylor series expansion is possible [27, 29]. Hence we have

$$J_i(\zeta) = n_i\, J(\zeta) = J_i(\xi) + \left.\frac{dJ_i(\zeta)}{d\zeta}\right|_{\zeta=\xi} \lambda + \mathcal{O}(\lambda^2) \tag{20}$$

and

$$J_1(\zeta) = \frac{dN^a(\zeta)}{d\zeta} x^a \tag{21}$$

$$J_2(\zeta) = \frac{dN^a(\zeta)}{d\zeta} y^a \tag{22}$$

where x^a and y^a represent the coordinates at the node a in the x and y directions, respectively.

The singularity $1/(z_m^\zeta - z_m^\xi)^2$ also has to be expanded in Taylor series. In this work, the expansion of $z_m^\zeta - z_m^\xi$ rather than $(z_m^\zeta - z_m^\xi)^2$ is used. The reason is that the expansion of the latter is more complicated and the same result can be achieved with the square of the expansion of the former. Thus we have

$$z_m^\zeta - z_m^\xi = \zeta_1 - \xi_1 + \mu_m(\zeta_2 - \xi_2) = \sum N^a(\zeta)x^a - \sum N^a(\xi)x^a + \mu_m\left(\sum N^a(\zeta)y^a - N^a(\xi)y^a\right) \tag{23}$$

Substituting Eq. (19) into (23) we obtain

$$z_m^\zeta - z_m^\xi = \left.\frac{dN^a(\zeta)}{d\zeta}\right|_{\zeta=\xi} \lambda\left(\sum x^a + \mu_m \sum y^a\right) = \Delta z\lambda \tag{24}$$

Finally, after substitution of Eqs. (19), (20) and (24) into (14), the regularised hypersingular integral is redefined as

$$\int_{-1}^{+1} s_{kij}^*(\zeta,\xi)N^a(\zeta)J(\zeta)d\zeta = \int_{-1}^{+1} G_0(\zeta,\xi)\,d\zeta + \int_{-1}^{+1}\frac{G_{-1}(\xi)}{\lambda}\,d\zeta + \int_{-1}^{+1}\frac{G_{-2}(\xi)}{\lambda^2}\,d\zeta \tag{25}$$

with

$$G_{-1}(\xi) = \frac{C_{kilr}}{\pi(\Delta z)^2}\Re\left\{B_{jm}Q_{ml}(\delta_{r1}+\mu_m\delta_{r2})(N^a(\xi)(J_1(\xi)'\mu_m - J_2(\xi)') + N^a(\xi)'(J_1(\xi)\mu_m - J_2(\xi)))\right\} \tag{26}$$

$$G_{-2}(\xi) = \frac{C_{kilr}}{\pi(\Delta z)^2}\Re\left\{N^a(\xi)B_{jm}Q_{ml}(\delta_{r1}+\mu_m\delta_{r2})(J_1(\xi)\mu_m - J_2(\xi))\right\} \tag{27}$$

where $(')$ denotes differentiation with respect to ζ.

Let us remark that during the evaluation of the Taylor series expansion in Eq. (25), terms with order $\mathcal{O}(\lambda^2)$ and higher do not contribute to the singular behaviour of the integrands. For this reason, they do not appear in Eqs. (26) and (27).

The same approach is used to regularise the strongly singular integrand from Eqs. (7) and (8), so further calculations will not be repeated here. The final expression of the regularised integral is given by

$$\int_{-1}^{+1} p_{ij}^*(\zeta,\xi)N^a(\zeta)J(\zeta)d\zeta = \int_{-1}^{+1} G_0(\zeta,\xi)\,d\zeta + \int_{-1}^{+1}\frac{G_{-1}(\xi)}{\lambda}\,d\zeta \tag{28}$$

with

$$G_{-1}(\xi) = \frac{1}{\pi\Delta z}\Re\left\{B_{jm}Q_{ml}N^a(\xi)(J_1(\xi)\mu_m - J_2(\xi))\right\} \tag{29}$$

To the best of the authors' knowledge, this regularisation scheme was not presented before for anisotropic materials and using the Stroh formalism.

4 The direct approach

Crack tip enrichment functions were first introduced in the BEM framework in the work of Simpson and Trevelyan [9], where isotropic enrichment functions were associated with the nodes of the elements containing the crack tip. It was shown that this type of enrichment is more general than using the quarter-point approach (see [30] for details of the quarter-point in a dual BEM formulation). Nevertheless, this type of strategy has the inconvenience of adding new degrees of freedom for every node that is enriched, which can significantly increase the condition number of the system.

An alternative was presented in the works of [10, 19], where the enrichment functions are embedded in the BIE. In this case, the Williams expansion was used to capture the asymptotic behaviour around the crack tip. The displacement field in the crack surfaces is defined in a similar way as in the work of Benzley [31],

$$u_j = \sum_{a=1}^{M} N^a u_j^a + \tilde{K}_I F_{Ij} + \tilde{K}_{II} F_{IIj} \tag{30}$$

where N^a represents the shape function for node a, u_j^a is a general coefficient rather than the nodal displacement, M is the number of nodes, $\tilde{K}_I$ and $\tilde{K}_{II}$ stand for the mode I and mode II SIF, respectively, and they are now part of the solution vector instead of being calculated after the displacement solution is obtained. In [10, 19], F_{Ij} and F_{IIj} are enrichment functions derived from the leading order term in the Williams expansion.

Adopting a polar coordinate system (r,θ) with origin at the crack tip, the asymptotic displacement field around a crack tip in a plane anisotropic domain can be expressed by means of the Stroh formalism [21] as

$$u_i(r,\theta) = \sqrt{\frac{2}{\pi}} \Re \left(K_\alpha A_{im} B_{m\alpha}^{-1} \sqrt{r\left(\cos\theta + \mu_m \sin\theta\right)} \right) \tag{31}$$

where the summation convention over repeated indices holds; $i,m = 1,2$; $\alpha = I, II$ is associated with the fracture modes. In the current paper, the enrichment functions F_{Ij} and F_{IIj} in (30) are obtained from the expansion and rearrangement of the terms of Eq. (31) in the same way as in [12], so that the enrichment functions are calculated as

$$F_{lj}(r,\theta) = \sqrt{\frac{2r}{\pi}} \begin{pmatrix} A_{11}B_{11}^{-1}\beta_1 + A_{12}B_{21}^{-1}\beta_2 & A_{11}B_{12}^{-1}\beta_1 + A_{12}B_{22}^{-1}\beta_2 \\ A_{21}B_{11}^{-1}\beta_1 + A_{22}B_{21}^{-1}\beta_2 & A_{21}B_{12}^{-1}\beta_1 + A_{22}B_{22}^{-1}\beta_2 \end{pmatrix} \tag{32}$$

where $\beta_i = \sqrt{\cos\theta + \mu_i \sin\theta}$, r is the distance between the crack tip and an arbitrary position, θ is the orientation measured from a coordinate system centred at the crack tip. Note that these enrichment functions are the equivalent of Williams expansion for isotropic materials [19].

The enriched DBIE and TBIE are defined as

$$c_{ij}(\boldsymbol{\xi})u_j(\boldsymbol{\xi}) + \int_\Gamma p^*_{ij}(\boldsymbol{\zeta},\boldsymbol{\xi})u_j(\boldsymbol{\zeta})d\Gamma(\boldsymbol{\zeta}) + \int_{\Gamma_c} p^*_{ij}(\boldsymbol{\zeta},\boldsymbol{\xi})\tilde{K}_{lj}F_{lj}(\boldsymbol{\xi})d\Gamma = \int_\Gamma u^*_{ij}(\boldsymbol{\zeta},\boldsymbol{\xi})p_j(\boldsymbol{\zeta})d\Gamma(\boldsymbol{\zeta}) \tag{33}$$

$$c_{ij}(\boldsymbol{\xi})p_j(\boldsymbol{\xi}) + N_k\int_\Gamma s^*_{kij}(\boldsymbol{\zeta},\boldsymbol{\xi})u_j(\boldsymbol{\zeta})d\Gamma(\boldsymbol{\zeta}) + N_k\int_{\Gamma_c} s^*_{kij}(\boldsymbol{\zeta},\boldsymbol{\xi})\tilde{K}_{lj}F_{lj}(\boldsymbol{\xi})d\Gamma = N_k\int_\Gamma d^*_{kij}(\boldsymbol{\zeta},\boldsymbol{\xi})p_j(\boldsymbol{\zeta})d\Gamma(\boldsymbol{\zeta}) \tag{34}$$

where Γ_c is the portion of the boundary Γ over which the enrichment is applied. Typically for an edge crack this might be the entire crack surfaces.

When the equations are discretised, $\tilde{K}_I$ and $\tilde{K}_{II}$ become part of the unknown vector. The main consequence is that the number of additional degrees of freedom is now fixed to two (for each crack tip), independent of the size of the enriched boundary. This represents a great advance compared to the number of additional degrees of freedom that are necessary in [9]. As well as reducing the size of the linear system, this restricted number of enrichment degrees of freedom has beneficial effects on conditioning.

The BIE containing the enrichment functions has singularities of the same order as discussed earlier for Eqs. (7) and (8). Therefore, the Guiggiani regularisation procedure is employed again. For the hypersingular enriched BIE, the regularisation terms are given by

$$G^{enr}_{-1}(\xi) = \frac{C_{kilr}}{\pi(\Delta z)^2}\Re\left\{B_{jm}Q_{ml}(\delta_{r1}+\mu_m\delta_{r2})(F_{lj}(\xi)(J_1(\xi)'\mu_m - J_2(\xi)') + F_{lj}(\xi)'(J_1(\xi)\mu_m - J_2(\xi)))\right\} \tag{35}$$

$$G^{enr}_{-2}(\xi) = \frac{C_{kilr}}{\pi(\Delta z)^2}\Re\left\{F_{lj}(\xi)B_{jm}Q_{ml}(\delta_{r1}+\mu_m\delta_{r2})(J_1(\xi)\mu_m - J_2(\xi))\right\} \tag{36}$$

and the regularisation terms of the strongly singular enriched BIE are given by

$$G^{enr}_{-1}(\xi) = \frac{1}{\pi\Delta z}\Re\left\{B_{jm}Q_{ml}F_{lj}(\xi)(J_1(\xi)\mu_m - J_2(\xi))\right\} \tag{37}$$

Since $\tilde{K}_I$ and $\tilde{K}_{II}$ are unknowns added to the linear system of equations, two more equations are required for the system of equations to be solved. As introduced by [19], these additional equations may come from a restriction in the crack faces, in order to remove the displacement discontinuity that may generally be observed at the crack tip when using discontinuous elements. The displacement continuity can be enforced by extrapolating, from a set of nodes on the upper and lower crack surfaces, to write an expression for the displacement at the crack tip. The resulting displacements are constrained to be identical, i.e.

$$\sum_{a=1}^{L} N^a u_j^{a\ upper} = \sum_{a=1}^{L} N^a u_j^{a\ lower} \tag{38}$$

where L is the number of nodes used for the crack tip extrapolation. Eq. (38) is applied for both x and y directions, resulting in two different equations. It should be noted that the extrapolation process is most accurate when taken over more than one element, i.e. L exceeds the number of nodes on a single element. The use of $L = 9$ with quadratic discontinuous elements has been found optimal in numerical tests.

5 Numerical results

In this section some numerical examples will be presented to validate the proposed direct evaluation approach. Reference solutions have been taken from the work of several authors. For instance, in reference [12], an 85×85 mesh is used with the geometrical enrichment approach. The fixed area enrichment is $r/a = 0.2$. The DBIE is used for discretisation of the external boundaries and the upper crack face, while the TBIE is used for the discretisation of the lower crack surface.

5.1 Crack in an infinite anisotropic domain

First, we analyse an infinite anisotropic domain subject to a uniform unidirectional loading in a direction perpendicular to a crack. This problem has a pure mode I exact solution of $K_I = \sigma_\infty \sqrt{\pi a}$, where σ_∞ represents the applied loading and a is the half-length of the crack. The problem is depicted in Figure 2.

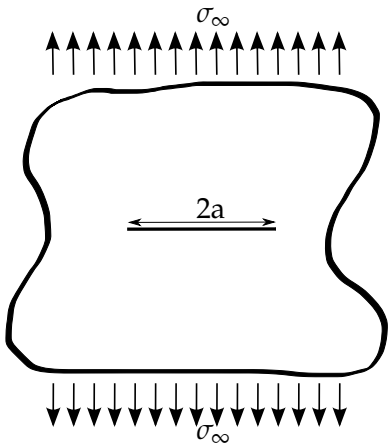

Figure 2: Crack in an infinite domain under uniform loading.

The crack is discretised with 8 discontinuous elements per crack surface. The material constants are given in the Voigt notation as: $C_{11} = 137.97$ GPa, $C_{12} = 5.78$ GPa, $C_{16} = 20.54$ GPa, $C_{22} = 12.45$ GPa, $C_{26} = 2.30$ GPa and $C_{66} = 12.98$ GPa.

Table 1 shows the percentage errors of K_I using (i) conventional, unenriched DBEM with the J-integral; (ii) unenriched DBEM with the extrapolation method; (iii) the enriched XBEM formulation using the direct SIF approach; (iv) the enriched XBEM with the J-integral; and (v) the enriched XBEM with the extrapolation method.

A modified version of the J-integral has been used for anisotropic materials, and is explained in detail in reference [32]. The extrapolation method consists of using the crack opening displacement (COD) and the crack relative sliding (CRS) to estimate the SIFs. The SIFs are thus given by [20]

$$\begin{pmatrix} K_{II} \\ K_I \end{pmatrix} = \sqrt{\frac{\pi}{8\overline{r}}} (\Re(i\mathbf{A}\mathbf{B}^{-1}))^{-1} \begin{pmatrix} \Delta u_1 \\ \Delta u_2 \end{pmatrix} \tag{39}$$

with $\overline{r} = L/6$, and L is the length of the element containing the crack tip.

Table 1: Results for the crack in an infinite anisotropic domain.

SIF calculation	$K_I = 1$	Error (%)
Unenriched J-integral	1.0296	2.9622
Unenriched Extrapolation	1.1554	15.5441
Direct SIF	1.0000	0.00115
Enriched J-integral	1.0240	2.4008
Enriched Extrapolation	0.9999	−0.00002

It is clear that the results obtained through the presence of the implicit enrichment are matching the exact solution. It is expected to have higher errors in the SIF extrapolation since there is no specific modelling of the asymptotic behaviour at the crack tip in this case. The results obtained with the enriched and non-enriched J-integral are practically identical.

The convergence is shown in Figure 3, where the SIF obtained with the direct approach is compared to the post-processed SIF calculated with the J-integral, for the non-enriched and enriched case. The results obtained with XBEM are very accurate even when the element size is large. The J-integral is converging to 0.98, which represents an error of 2%. One can verify that the enriched J-integral shows slightly better results than the non-enriched J-integral.

The high accuracy obtained on a coarse mesh should come as no surprise, since it is the enrichment, rather than piecewise polynomial functions, that are principally responsible for capturing the solution around the crack tip.

5.2 Orthotropic plate with a centred crack

Figure 4 shows a rectangular orthotropic plate, of dimensions $2h \times 2w$, with a centred crack subject to a uniform loading. Here we consider the case of a

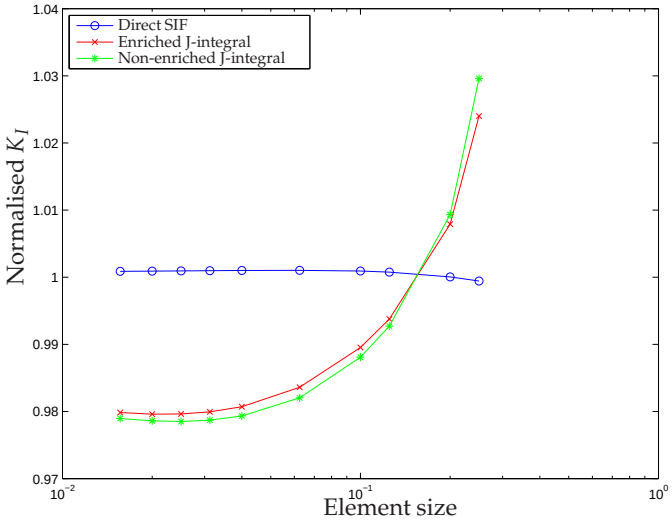

Figure 3: Convergence of the mode I SIF with respect to the element size.

square plate, i.e. $h/w = 1$. The crack length is defined such that $a/w = 0.2$. The material properties in this example are given by: $\nu_{12} = 0.03$, $G_{12} = 6$ GPa, and E_1 and E_2 are defined in terms of the parameter ϕ

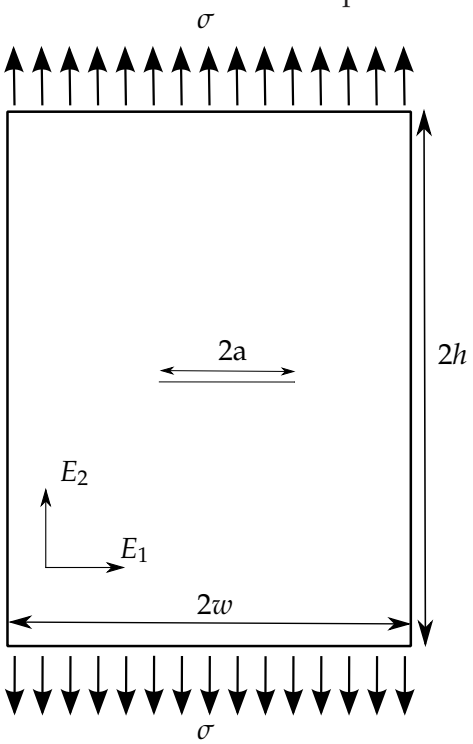

Figure 4: Centred crack in an orthotropic plate.

$$E_1 = G_{12}(\phi + 2\nu_{12} + 1) \tag{40}$$

$$E_2 = \frac{E_1}{\phi} \tag{41}$$

The direct SIF method is compared with an XFEM formulation with orthotropic enrichment functions [33], an XFEM formulation with fully anisotropic enrichment functions [12] and a BEM formulation [24]. A 85×85 mesh was employed with the XFEM formulation from [33]. The BEM mesh used 24 continuous elements on the external boundary and 10 discontinuous elements on the crack surfaces.

Figure 5 shows the results for the normalised mode I SIF in terms of the parameter ϕ. One can verify that the direct approach and the XFEM from [12] present good agreement, while the BEM and XFEM from [33] appear to be overestimating the SIF when $\phi > 0.7$.

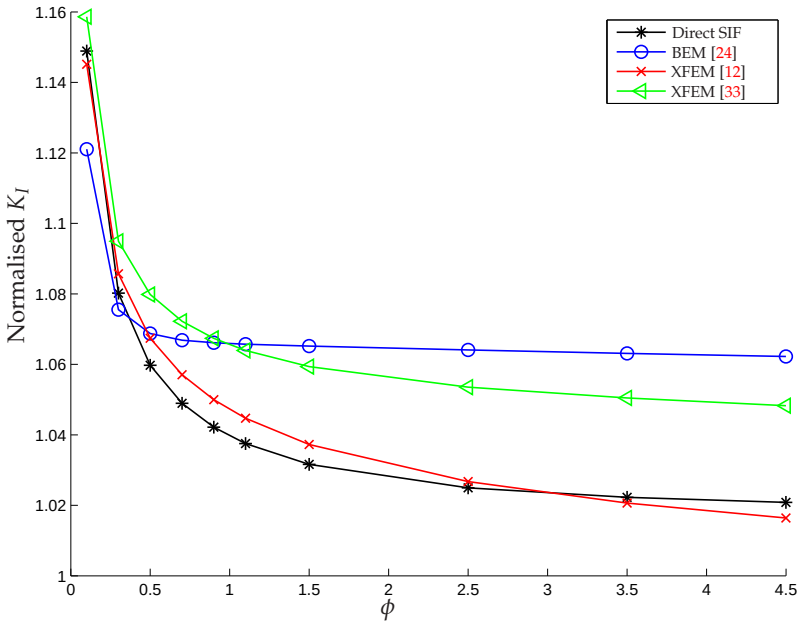

Figure 5: Normalised mode I SIF for the orthotropic centred crack.

5.3 Anisotropic plate with double edge crack

In this example, a square plate ($h/w = 1$) with edge cracks in both left and right sides is analysed. The crack length is obtained from $a/w = 0.5$. A uniform load is applied in the upper and lower surfaces. Figure 6 illustrates the problem.

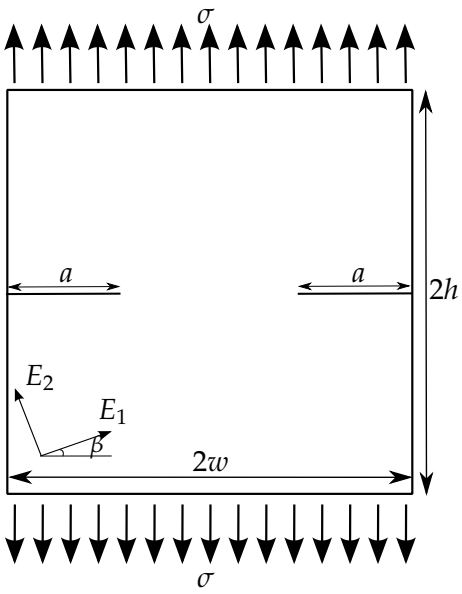

Figure 6: Double edge crack in an anisotropic plate.

The plate is a symmetric angle ply composite laminate of four graphite-epoxy laminae, with the following elastic properties: $E_1 = 144.8$ GPa, $E_2 = 11.7$ GPa, $G_{12} = 9.66$ GPa and $\nu_{12} = 0.21$. The fibre is rotated from $\phi = 0°$ to $\phi = 90°$ and SIFs calculated.

The BEM mesh contains 24 discontinuous elements on the external boundaries and 16 discontinuous elements on the crack surfaces. Figure 7 shows the normalised mode I SIF for the proposed approach and some reference solutions. Excellent agreement with the solution from reference [34] is achieved. The solution from reference [24] seems to be underestimating the SIFs for $30° \leq \beta < 70°$. The solutions obtained with the anisotropic J-integral are the same for both unenriched and enriched cases. The extrapolation method only provides a meaningful solution when the enrichment is present.

5.4 Anisotropic plate with slanted centred crack

A rectangular ($h/w = 2$) composite laminate with a centred crack under a uniform loading is shown in Figure 8. The angle θ represents the orientation of the crack, while β represents the rotation of the fibres with respect to the principal axis. The crack length is defined as: $2a = 0.4w$. The material properties of the laminate are given by: $E_1 = 48.26$ GPa, $E_2 = 17.24$ GPa, $G_{12} = 6.89$ GPa, $\nu_{12} = 0.29$. In this example, $\theta = 45°$.

The external boundary is discretised with 36 continuous elements and the crack surfaces with 10 discontinuous elements. Figures 9 and 10 represent the normalised mode I and II, respectively, of the direct approach and BEM reference solutions from [24] and [35] and the XFEM solution from

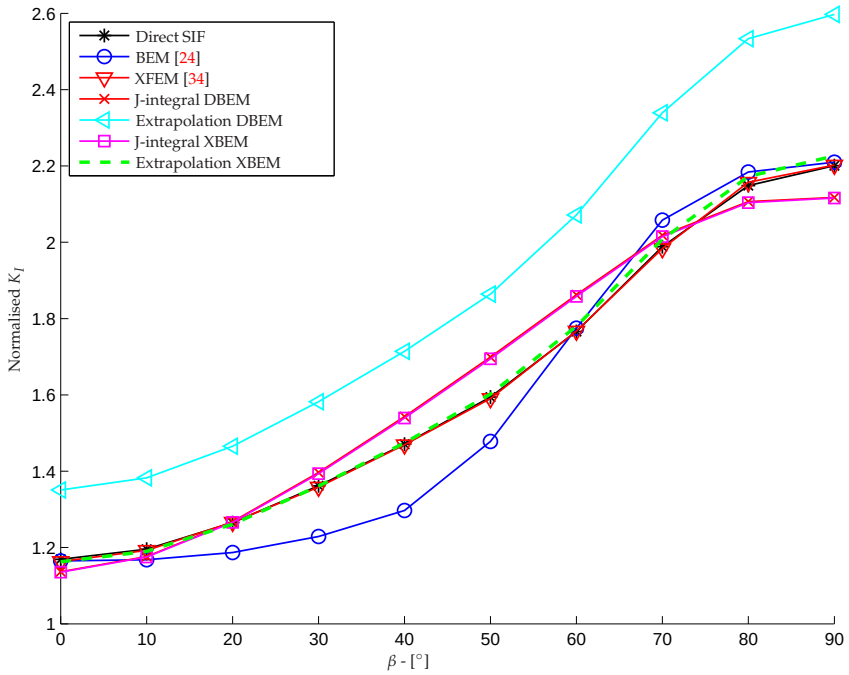

Figure 7: Normalised mode I SIF for the anisotropic double edge crack.

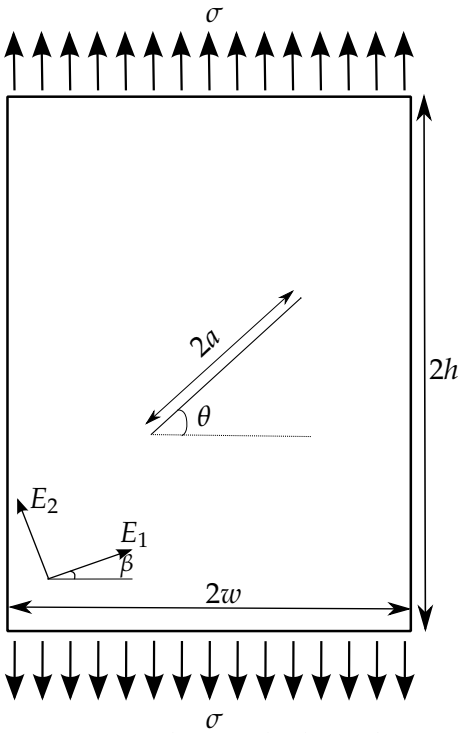

Figure 8: Anisotropic plate with slanted centred crack.

[12]. Good agreement is attained with both XFEM and BEM reference solutions.

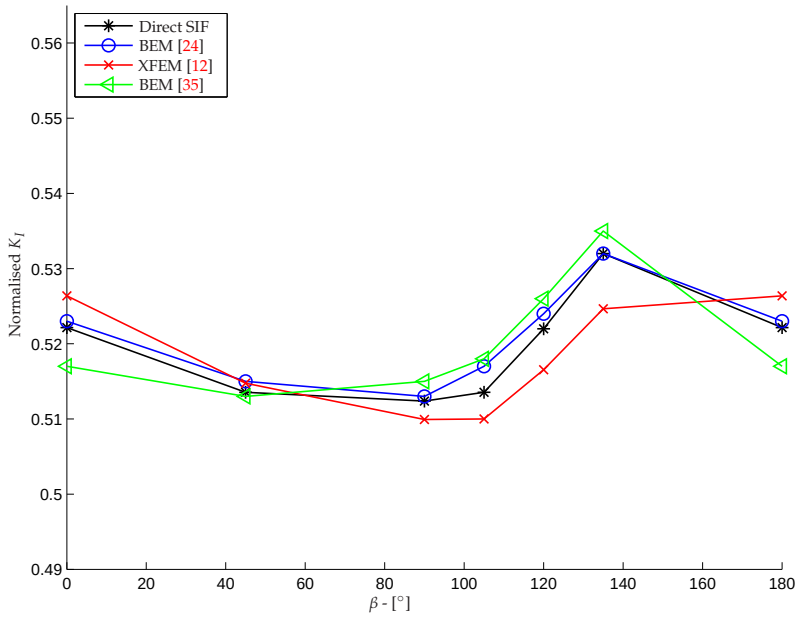

Figure 9: Normalised mode I SIF for the anisotropic centred crack ($\theta = 45°$).

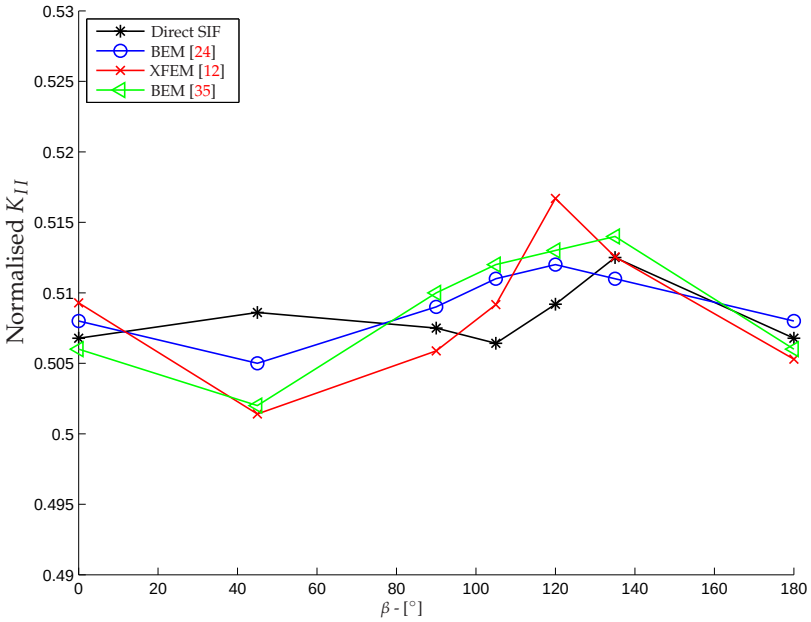

Figure 10: Normalised mode II SIF for the anisotropic centred crack ($\theta = 45°$).

5.5 Cracks emerging from a hole

A rectangular plate ($h/w = 2$) with two cracks emerging from a hole is shown in Figure 11. The diameter of the hole is fixed at $r/w = 0.5$ and $0.55 \leq a/r \leq 0.7$. The plate is an unidirectional boron-epoxy composite laminate presenting the following material properties: $E_1 = 204$ GPa, $E_2 = 18.5$ GPa, $G_{12} = 5.59$ GPa and $\nu_{12} = 0.23$. The anisotropy of the plate is achieved through variation of the fibre orientation ϕ from 0° to 90°.

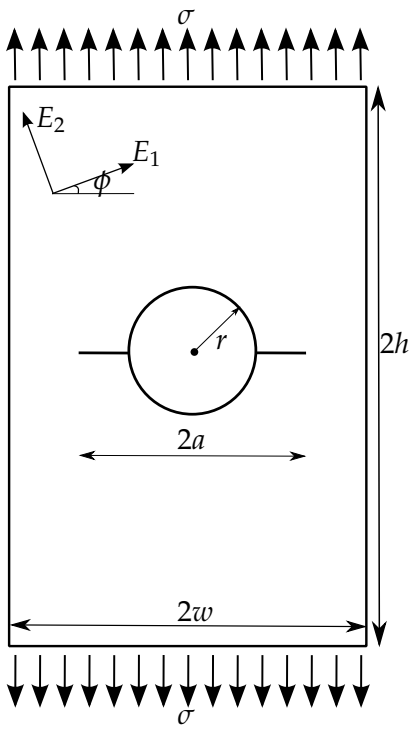

Figure 11: Cracks emerging from a hole.

The BEM meshes consist of 34 continuous elements on the external boundaries, 28 continuous elements on the hole and 5 elements on the crack surfaces. Figures 12 and 13 illustrate the results for the normalised mode I and mode II, respectively. Good agreement with the reference solution is achieved in both cases.

6 Summary

A direct evaluation of the SIF for problems in linear elastic fracture mechanics in anisotropic materials has been proposed. The Stroh formalism has been used as the fundamental solution of a dual BEM formulation and in the expression of the asymptotic behaviour of the anisotropic materials around the crack tip. A concise and orientation-free enrichment function

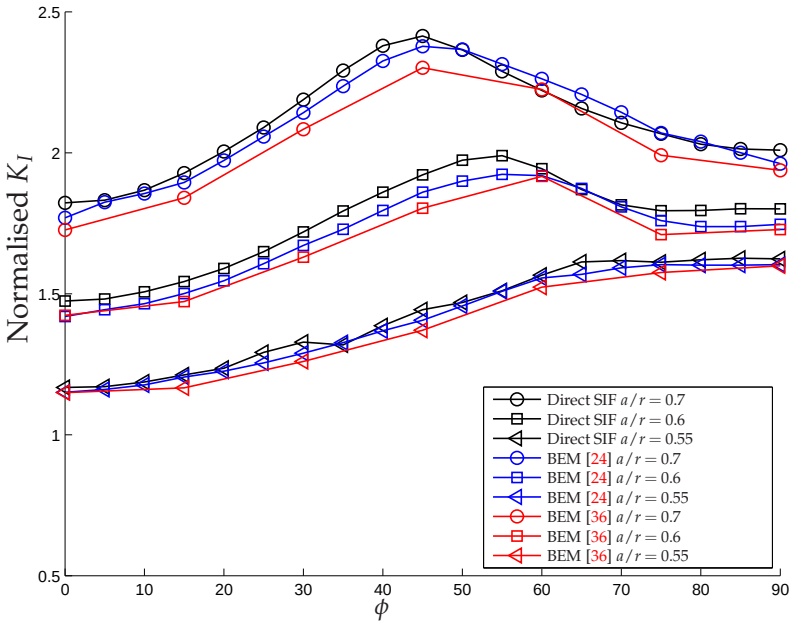

Figure 12: Normalised mode I SIF for the crack emerging from a hole.

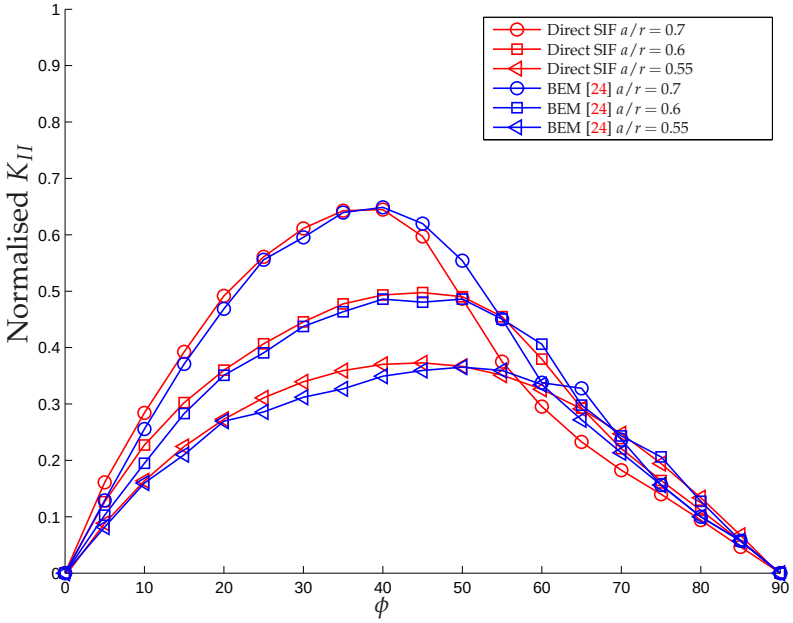

Figure 13: Normalised mode II SIF for the crack emerging from a hole.

is obtained, which depends only on the material properties. The Guiggiani method for regularising singular and hypersingular kernels has been used for the first time for anisotropic materials with the Stroh formalism for both

singularities of the regular kernels from the BEM formulation as well as in the application of these kernels in the integrals containing the enrichment functions. Several examples have been presented comparing the proposed methodology with other BEM and XFEM solutions, and good agreement has been found between them. Furthermore, the approach could be extended to 3D, and this is work in progress. At each location on the crack front, an enrichment based on the plane strain asymptotic displacement can be applied in the plane perpendicular to the crack front.

Acknowledgements

The first author acknowledges the Faculty of Science, Durham University for his Postdoctoral Research Associate funding. The second author is supported by the Ministry of Education of Saudi Arabia under Ref. No. S11973.

References

[1] Babuška I, Melenk JM. The partition of unity method. *International Journal for Numerical Methods in Engineering* 1997; **4**:607–632.

[2] Belytschko T, Black T. Elastic crack growth in finite elements with minimal remeshing. *International Journal for Numerical Methods in Engineering* 1999; **45**:601–620.

[3] Möes N, Dolbow J, Belytschko T. A finite element method for crack growth without remeshing. *International Journal for Numerical Methods in Engineering* 1999; **46**(1):131–150.

[4] Chevaugeon N, Möes N, Minnebo H. Improved crack tip enrichment functions and integration for crack modeling using the extended finite element method. *International Journal for Multiscale Computational Engineering* 2013; **11**(6):597–631, doi:10.1615/IntJMultCompEng.2013006523.

[5] Gordeliy E, Peirce A. Enrichment strategies and convergence properties of the XFEM for hydraulic fracture problems. *Computer Methods in Applied Mechanics and Engineering* 2015; **283**:474–502, doi:10.1016/j.cma.2014.09.004.

[6] Nasirmanesh A, Mohammadi S. XFEM buckling analysis of cracked composite plates. *Composite Structures* 2015; **131**:333–343, doi:10.1016/j.compstruct.2015.05.013.

[7] Raschetnia R, Mohammadi S. Finite strain fracture analysis using the extended finite element method with new set of enrichment functions. *International Journal for Numerical Methods in Engineering* 2015; **102**:1316–1351.

[8] Zhu QZ. On enrichment functions in the extended finite element method. *International Journal for Numerical Methods in Engineering* 2012; **91**:186–217.

[9] Simpson R, Trevelyan J. A partition of unity enriched dual boundary element method for accurate computations in fracture mechanics. *Computer Methods in Applied Mechanics and Engineering* 2011; **200**(1):1–10.

[10] Simpson R, Trevelyan J. Evaluation of J_1 and J_2 integrals for curved cracks using an enriched boundary element method. *Engineering Fracture Mechanics* 2011; **78**(4):623–637.

[11] Laborde P, Pommier J, Renard Y, Salaün M. High-order extended finite element method for cracked domains. *International Journal for Numerical Methods in Engineering* 2005; **64**:354–381.

[12] Hattori G, Rojas-Díaz R, Sáez A, Sukumar N, García-Sánchez F. New anisotropic crack-tip enrichment functions for the extended finite element method. *Computational Mechanics* 2012; **50**(5):591–601.

[13] Béchet E, Minnebo H, Moës N, Burgardt B. Improved implementation and robustness study of the X-FEM for stress analysis around cracks. *International Journal for Numerical Methods in Engineering* 2005; **64**(8):1033–1056.

[14] Liu XY, Xiao QZ, Karihaloo BL. XFEM for direct evaluation of mixed mode SIFs in homogeneous and bi-materials. *International Journal for Numerical Methods in Engineering* 2004; **59**(8):1103–1118.

[15] Xiao QZ, Karihaloo BL, Liu XY. Direct determination of SIF and higher order terms of mixed mode cracks by a hybrid crack element. *International Journal of Fracture* 2004; **125**(3-4):207–225.

[16] Li S, Mear M, Xiao L. Symmetric weak-form integral equation method for three-dimensional fracture analysis. *Computer Methods in Applied Mechanics and Engineering* 1998; **151**(3):435–459.

[17] Watson J. Singular boundary elements for the analysis of cracks in plane strain. *International Journal for Numerical Methods in Engineering* 1995; **38**:2389–2411.

[18] Portela A, Aliabadi MH, Rooke DP. Efficient boundary element analysis of sharp notched plates. *International Journal for Numerical Methods in Engineering* 1991; **32**:445–470.

[19] Alatawi IA, Trevelyan J. A direct evaluation of stress intensity factors using the extended dual boundary element method. *Engineering Analysis with Boundary Elements* 2015; **52**:56–63.

[20] García-Sánchez F, Sáez A, Domínguez J. Anisotropic and piezoelectric materials fracture analysis by BEM. *Computers & Structures* 2005; **83**(10):804–820.

[21] Suo Z. Singularities, interfaces and cracks in dissimilar anisotropic media. *Proceedings of the Royal Society of London. Series A, Mathematical and Physical Sciences* 1990; **427**(1873):331–358.

[22] Stroh AN. Dislocation and cracks in anisotropic elasticity. *Philosophical magazine* 1958; **3**:625–646.

[23] Ting TCT. *Anisotropic Elasticity*. Oxford University Press, New York, 1996.

[24] García-Sánchez F, Sáez A, Domínguez J. Traction boundary elements for cracks in anisotropic solids. *Engineering Analysis with Boundary Elements* 2004; **28**(6):667–676.

[25] Telles JCF. A self-adaptive co-ordinate transformation for efficient numerical evaluation of general boundary element integrals. *International Journal for Numerical Methods in Engineering* 1987; **24**(5):959–973.

[26] Guiggiani M, Casalini P. Direct computation of Cauchy principal value integrals in advanced boundary elements. *International Journal for Numerical Methods in Engineering* 1987; **24**:1711–1720.

[27] Guiggiani M, Krishnasamy G, Rudolphi TJ, Rizzo FJ. A general algorithm for the numerical solution of hypersingular boundary integral equations. *Journal of applied mechanics* 1992; **59**(3):604–614.

[28] Guiggiani M. Formulation and numerical treatment of boundary integral equations with hypersingular kernels. *Singular integrals in boundary element methods* 1998; :85–124.

[29] Aliabadi M, Hall W, Phemister T. Taylor expansions for singular kernels in the boundary element method. *International Journal for Numerical Methods in Engineering* 1985; **21**(12):2221–2236.

[30] Sáez A, Gallego R, Domínguez J. Hypersingular quarter-point boundary elements for crack problems. *International Journal for Numerical Methods in Engineering* 1995; **38**:1681–1701.

[31] Benzley SE. Representation of singularities with isoparametric finite elements. *International Journal for Numerical Methods in Engineering* 1974; **8**(3):537–545.

[32] Sollero P, Aliabadi MH. Fracture mechanics analysis of anisotropic plates by the boundary element method. *International Journal of Fracture* 1993; **64**(4):269–284.

[33] Asadpoure A, Mohammadi S. Developing new enrichment functions for crack simulation in orthotropic media by the extended finite element method. *International Journal for Numerical Methods in Engineering* 2007; **69**(10):2150–2172.

[34] Natarajan S, Song C. Representation of singular fields without asymptotic enrichment in the extended finite element method. *International Journal for Numerical Methods in Engineering* 2013; **96**:813–841.

[35] Sollero P, Aliabadi MH. Anisotropic analysis of cracks in composite laminates using the dual boundary element method. *Composite structures* 1995; **31**(3):229–233.

[36] Sollero P, Aliabadi MH, Rooke DP. Anisotropic analysis of cracks emanating from circular holes in composite laminates using the boundary element method. *Engineering Fracture Mechanics* 1994; **49**(2):213–224.